ACS APPLIED MATERIALS & INTERFACES

www.acsami.org

Research Article

Ce-MOF@Au-Based Electrochemical Immunosensor for Apolipoprotein A1 Detection Using Nanobody Technology

Baihe Sun,[⊥] Guanghui Li,[⊥] Yue Wu, Junwei Gai, Min Zhu, Weiwei Ji, Xiaoying Wang, Fenghua Zhang, Wanting Li, Jingjin Hu, Yuxin Lou, Gusheng Feng, Xijun Han, Jinwen Dong, Jiayuan Peng, Jiawei Pei, Yakun Wan,* Yanfei Li,* and Linlin Ma*

Cite This: https://doi.org/10.1021/acsami.4c14027

Read Online

ACCESS | Metrics & More | Article Recommendations | Supporting Information

ABSTRACT: Apolipoprotein A1 (Apo-A1) is a well-recognized biomarker in tissues, closely associated with cardiovascular diseases such as atherosclerosis, coronary artery disease, and heart failure. However, existing methods for Apo-A1 determination are limited by costly equipment and intricate operational procedures. Given the distinct advantages of electrochemical immunosensors, including affordability and high sensitivity, along with the unique attributes of nanobodies (Nbs), such as enhanced specificity and better tissue permeability, we developed an electrochemical immunosensor for Apo-A1 detection utilizing Nb technology. In our study, Ce-MOF@AuNPs nanocomposites were synthesized by using ultrasonic methods and applied to modify a glassy carbon electrode. The Nb6, screened from an Apo-A1 immunized phage library, was immobilized onto the nanocomposite material, establishing a robust binding interaction with Apo-A1. The recorded peak current values demonstrated a logarithmic increase corresponding to Apo-A1 concentrations ranging from 1 to 100,000 pg/mL, with a detection limit of 36 fg/mL. Additionally, the developed immunosensors demonstrated high selectivity, good stability, and reproducibility. Our methodology was also effectively utilized for serum sample analysis, showing good performance in clinical assessments. This electrochemical immunosensor represents a promising tool for Apo-A1 detection, with significant potential for advancing cardiovascular disease diagnostics.

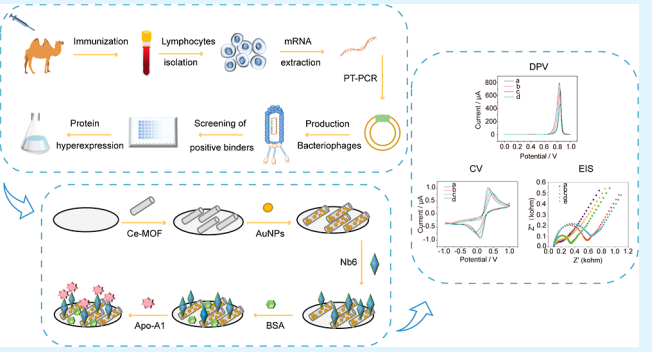

KEYWORDS: *nanobody, apolipoprotein A1, metal−organic framework, gold nanoparticles, electrochemical sensor*

INTRODUCTION

Apolipoprotein A1 (Apo-A1) functions as a pivotal protein in high-density lipoprotein (HDL) and is essential for the antiatherosclerotic activity of HDL.[1] Elevated levels of Apo-A1 are commonly observed in tissues and exhibit an inverse correlation with the occurrence of atherosclerosis and coronary heart disease.[2,3] It facilitates the early identification of coronary heart disease risk and serves as a biomarker for monitoring lipid-modifying drug therapy.[4] Previous studies have demonstrated that reduced Apo-A1 levels are associated with left ventricular dysfunction, with further evidence indicating a strong correlation between lower Apo-A1 concentrations and adverse prognoses in individuals with nonischemic heart failure.[5,6] Current quantification techniques for Apo-A1, such as enzyme-linked immunosorbent assays (ELISA),[7−9] immunoturbidimetric analysis,[10,11] and LC−MS/MS,[12,13] often suffer from limitations, including complex sample preparation or intricate operational procedures. In contrast, electrochemical methods have gained popularity in immunosensor detection due to their enhanced sensitivity, superior accuracy, and cost-effectiveness.[14−18] These sensors enable rapid and precise detection of Apo-A1 and other cardiovascular disease markers, including proteins, DNA, and enzymes, in blood samples. Unlike ELISA, which has a sensitivity threshold at the nanogram per milliliter level,[19] electrochemical sensors demonstrate greater sensitivity. Additionally, label-free electrochemical sensors, detecting antigens without markers, are frequently used in sensor development due to their simplified measurement techniques and procedures.

Metal−organic frameworks (MOFs), belonging to a novel category of porous materials consisting of metal ions and organic ligands, are extensively applied in sensor fabrication due to their adjustable pore size, robust adsorption capacity, and commendable biocompatibility.[20] More importantly,

Received: August 20, 2024
Revised: October 2, 2024
Accepted: October 6, 2024

MOFs are commonly used for the immobilization of functional molecules due to their excellent adsorption and adhesion properties. Previous studies have indicated that Ce-MOF holds significant potential in bioanalysis,[21] with its large specific surface area and outstanding optical, electrochemical, and catalytic properties. These attributes make Ce-MOFs ideal materials for electrode modification. Additionally, the synthesis of Ce-MOFs using benzenetricarboxylic acid as the organic framework is also efficient and straightforward, further improving the feasibility of sensor construction.[21] Moreover, gold nanoparticles (AuNPs) enhance the electrical conductivity of the electrodes, increase the specific surface area of the materials, and exhibit excellent biocompatibility.[22] AuNPs can covalently bond with antibodies, thereby improving their immobilization. Integrating Ce-MOFs with AuNPs enables the comprehensive utilization of the electrochemical catalytic activity inherent to AuNPs, while leveraging the selective adsorption properties of Ce-MOF materials.[23,24] In this study, AuNPs were deposited on the surface of Ce-MOFs to form a layered structure, which heightened the sensitivity and selectiveness for Apo-A1 detection. We combined Ce-MOF@Au nanomaterials with high-specificity and high-affinity nanobodies (Nbs) to target the novel biomarker Apo-A1. By monitoring changes in electrochemical signals, our study successfully achieved rapid and precise detection of both the presence and concentration of Apo-A1.

In clinical analysis, mAbs are regarded as the gold standard for immunoassays. However, issues such as batch-to-batch variability, high production costs, and the large molecular weight of mAbs, limiting their sensitivity in impedance assays, highlight the need to explore alternative bioreceptors.[25] Nbs, also known as the variable domain of the heavy-chain antibody (VHH, ~2.5 × 3 × 4 nm),[26,27] are the smallest antibody fragments proficient in antigen binding, with a molecular weight of approximately 15 kDa.[28,29] Compared to mAbs, Nbs possess unique properties, including elevated selectivity,[30,31] higher affinity,[31] superior thermal stability,[32] and the singular attribute of a single structural domain.[33] As a structural domain with a single intrachain disulfide bond, Nbs exhibit remarkable structural stability and can tolerate extreme conditions such as high temperatures and acidic and alkaline environments. For example, they retain high antigen-binding activity even after storage at 37 °C for several weeks and can endure temperatures ranging from 60 to 80 °C.[34] Due to its small size, Nbs can be immobilized at a higher density on the immunosensor compared to conventional antibodies, improving the signal-to-noise ratio.[35] This enhancement lowers the limit of detection (LOD) and facilitates sensitive antigen analysis, making Nbs a promising alternative to traditional antibodies in electrochemical point-of-care technologies.[36] Nbs are now widely utilized in diagnostic kits and procedures for detecting pathogens, cancer, and other biomarkers.[37,38]

In this study, we successfully screened Nbs specific to Apo-A1, confirming their high affinity. Ce-MOF@Au nanocomposites, which attract negatively charged AuNPs, leverage the excellent electrical conductivity of AuNPs to enhance the electron transport across the electrodes. Additionally, using a label-free approach simplifies both the measurement process and the procedure. We present, for the first time, the application of Ce-MOF@Au for Apo-A1 detection. This study also represents the first integration of Ce-MOF@Au with Nbs in an electrochemical sensing platform. A comprehensive performance evaluation confirmed the sensor's reliability and effectiveness. Compared with conventional immunosensors, our approach offers a substantial reduction in cost while maintaining comparable detection limits, thus enhancing economic feasibility. In conclusion, the label-free electrochemical immunosensor utilizing Ce-MOF@Au multilayer nanocomposites offers a robust and cost-effective analytical technique for Apo-A1 detection.

EXPERIMENTAL SECTION

Materials and Reagents. Cerium(III)nitrate hexahydrate, trimesic acid, terephthalic acid, hydrogen tetrachloroaurate(III)-trihydrate, albumin, and sodium citrate were supplied by damas-beta; potassium ferricyanide, potassium ferrocyanide trihydrate, uric acid, cholesterol, bilirubin, sodium borohydride solution, creatinine, urea, and potassium chloride were all purchased from Aladdin (Shanghai, China, www.aladdin-e.com), Human Apo-A1 ELISA Kit was purchased from EIAab (Wuhan, China).

Immunization and Library Construction. A juvenile and robust Bactrian camel underwent initial immunization with Apo-A1, in conjunction with an equivalent volume of Freund's complete adjuvant (Sigma-Aldrich, St. Louis, MO, USA). Subsequently, the camel received regular weekly immunizations employing Freund's incomplete adjuvant (Sigma-Aldrich).

After the seventh immunization, peripheral blood lymphocytes were extracted from 100 mL of camel blood utilizing Ficoll−Paque PLUS (GE Healthcare, Pittsburgh, PA, USA). Subsequently, a phage display library containing genes encoding Nbs was constructed using established methodologies.[39,40] The library's capacity and the ratio of correct insertions were assessed to determine the colony-forming units (CFUs). All experimental procedures were conducted in strict adherence to the guidelines set forth by the National Institutes of Health for the ethical care and utilization of laboratory animals.

Screening of Apo-A1-specific Nbs by Phage Display Technology. Nbs specific to human Apo-A1 were screened using a combination of phage display and Periplasmic Extract ELISA (PE-ELISA), following established procedures as previously documented.[41,42] After the sequencing of the selected clones, which were chosen as representatives of distinct families of Apo-A1-specific Nbs, the selection criteria were based on their possession of diverse amino acid sequences within complementarity-determining region 3 (CDR3). Anti-Apo-A1 Nbs were primarily expressed in *Escherichia coli* and subsequently purified using protein A affinity chromatography (Qiagen, Germany). The purity of the Nbs was evaluated through SDS−PAGE analysis.

Affinity Determination. The kinetics of Nbs anti-Apo-A1 antigen were examined through biolayer interferometry (BLI) using a Fortebio's Octet RED96 instrument (ForteBio, Menlo Park, CA, USA). Briefly, Nbs (10 μg/mL) were diluted and immobilized on protein A biosensors followed by incubation with serially diluted Apo-A1. The subsequent dissociation phase was carried out in PBST. The obtained binding curves were fitted using the 1:1 binding model with Octet Data Analysis software, version 9.0. Tracking of the association and dissociation rates enabled the determination of the equilibrium dissociation constant (K_D). This comprehensive approach allowed for a detailed investigation of the dynamic binding interactions between Nbs and the Apo-A1 antigen.

Synthesis of Ce-MOF. Initially, 266.64 μM trimesic acid was dissolved in 30 mL of ethanol, and concurrently, 266.68 μM $Ce(NO_3)6H_2O$ was dissolved in 30 mL of Milli-Q water. The solution containing trimesic acid was then introduced into the $Ce(NO_3)6H_2O$ solution, followed by stirring for 30 min. The resulting white mixture underwent ultrasonication for an additional 30 min and underwent three successive washes with Milli-Q water and ethanol. The resultant material was subsequently dried at 70 °C to obtain the Ce-MOF.

Synthesis of Ce-MOF@Au. The synthesis of AuNPs commenced with the preparation of a 1% trisodium citrate solution. This was achieved by dissolving 200 mg of trisodium citrate in 20 mL of Milli-Q water. Subsequently, 457.05 μM $HAuCl_4$ was measured and added

https://doi.org/10.1021/acsami.4c14027
ACS Appl. Mater. Interfaces XXXX, XXX, XXX−XXX

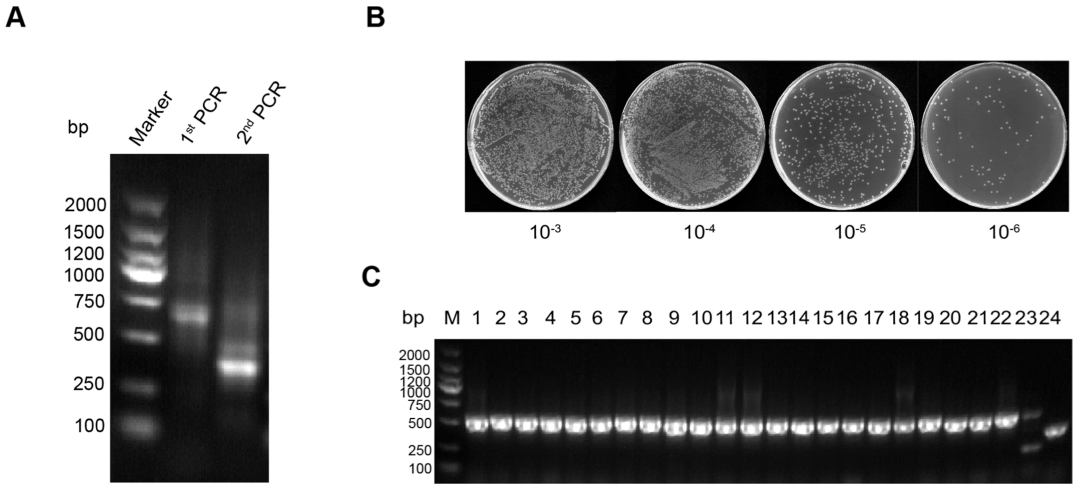

Figure 1. Construction of anti-Apo-A1 Nbs phage-displayed library. (A) The segments harboring VHH gene fragments underwent amplification through an initial PCR followed by a nested PCR. (B) The library capacity was assessed by counting the clones on plates after gradient dilution. (C) The accurate insertion rate of the library was determined by conducting PCR on a randomly selected set of 24 colonies.

to 200 mL of boiling water. Following this, 15 mL of a 1% trisodium citrate solution was introduced into the $HAuCl_4$ solution. Concurrently, a 1 mg/mL solution of Ce-MOF was prepared and dissolved in Milli-Q water. The resulting solution was stirred for 4 h, subjected to centrifugation, and subsequently washed three times.[21]

Preparation of Electrochemical Immunosensor. The glassy carbon electrode (GCE) was initially polished using 0.3 and 0.05 μm alumina powder, followed by sonication in absolute Milli-Q water, ethanol, and Milli-Q water to achieve a smooth interface. After air-drying at room temperature, GCE underwent modification with the Ce-MOF@Au nanocomposites. Subsequently, 10 μL of anti-Apo-A1 Nb solution (10 μg/mL) was carefully deposited onto the surface of the modified electrode and allowed to incubate for 12 h at 4 °C to facilitate the immobilization of Nbs. Any unbound Nbs were thoroughly washed away using a 0.01 M PBS. Following this, 5 μL of 1% BSA solution was applied onto the modified electrode and allowed to incubate for 30 min to block nonspecific binding sites. Subsequently, any unbound BSA was thoroughly washed away using 0.01 M PBS. Finally, the modified electrode was subjected to incubation in various antigen concentrations for 40 min at 37 °C, facilitating the establishment of a label-free electrochemical immunosensor.

Morphology Characterization of Materials. The morphologies were examined using a scanning electron microscope (SEM, Hi High-Technologies, Regulus 8100) operating at an accelerating voltage of 10 kV. Additionally, a transmission electron microscope (TEM, JEM-F200) was employed with an acceleration voltage of 200 kV. For TEM analysis, the materials were ultrasonically dispersed in an aqueous solution, drop-coated onto an ultrathin carbon film, dried, and subsequently analyzed using a JEM-2100F instrument. For SEM analysis, the material was ultrasonically dispersed in an aqueous solution, coated onto a silicon wafer, dried, gold-sputtered for 30 s, and then characterized by using SEM on a Regulus 8100 instrument.

Electrochemical Measurements with Ce-MOF@Au/GCEs. The electrochemical investigations were conducted employing a conventional three-electrode system comprising a GCE as the working electrode, a Ag/AgCl electrode as the reference electrode, and a platinum wire as the counter electrode. Electrochemical analyses, encompassing differential pulse voltammetry (DPV), cyclic voltammetry (CV), and electrochemical impedance spectroscopy (EIS), were conducted by utilizing a CHI760E electrochemical workstation. The current and potential characteristics of Ce-MOF@Au were measured using DPV. Within a 0.2 M PBS solution (pH 7.3), the scan potential spanned from −1 to 1 V, with a scan rate of 0.1 V/s. The pulse width and period were set at 0.0167 and 0.5 s, respectively.[23] The CV experiments were conducted with potentials ranging from −1 to +1 V at a scan rate of 100 mV/s. The EIS measurements were performed across a frequency range of 10^{-1} to 10^6 Hz. Both determinations were evaluated in a solution containing 5 mmol/L $[Fe(CN)_6]^{-3/-4}$ and 0.1 mol/L KCl.

Human serum samples were diluted 50,000 times with 0.01 M PBS, and quantified using a conventional human Apo-A1 ELISA kit. Subsequently, the serum was diluted 50,000 times with 0.01 M PBS and directly analyzed using Ce-MOF@Au sensors. The procedures were conducted in accordance with the principles outlined in the Declaration of Helsinki regarding biomedical research involving human subjects.

RESULTS AND DISCUSSION

Anti-Apo-A1 Nb Phage Display Library Construction. To establish the anti-Apo-A1 Nb phage display library, we initially immunized a young and healthy camel with Apo-A1. Subsequently, VHH genes were amplified from cDNA, which was reverse transcribed from lymphocyte RNA after 7 times of immunization. The initial PCR yielded distinct bands at approximately 700 bp, as depicted in Figure 1A first PCR. The VHH-only fragments were obtained by amplifying from the 700 bp fragments as templates, resulting in a final band size of approximately 400 bp, as illustrated in Figure 1A second PCR. The recombinant pMECS-VHH vector was electro-transformed into TG1 cells, and both the inset ratio and library capacity were accessed. The library size was determined to be 5 × 10^9 CFU through gradient dilutions (Figure 1B), with a correct insertion ratio of 91.6% (Figure 1C). The substantial library capacity supports the efficient isolation of specific Nbs against Apo-A1. In summary, we successfully established a phage-displayed immune VHH library in preparation for the subsequent selection of anti-Apo-A1 Nbs.

Apo-A1-specific Nbs was Screened through Phage Display Technology and Affinity Analysis. In this study, we employed phage display technology to screen specific anti-Apo-A1 Nbs. The quantification of phage particle enrichment was assessed by comparing the elution from Apo-A1-coated wells to that from uncoated wells. The enrichment increased to 24.4-fold by the third round of biopanning (Figure 2A), indicating a promising likelihood of isolating high specificity anti-Apo-A1 Nbs. Moreover, PE-ELISA analysis identified 23 positive clones with a binding ratio exceeding 3 from 96 randomly selected clones (Figure 2B). DNA sequencing determined six Nbs with distinct amino acid sequences in

https://doi.org/10.1021/acsami.4c14027
ACS Appl. Mater. Interfaces XXXX, XXX, XXX−XXX

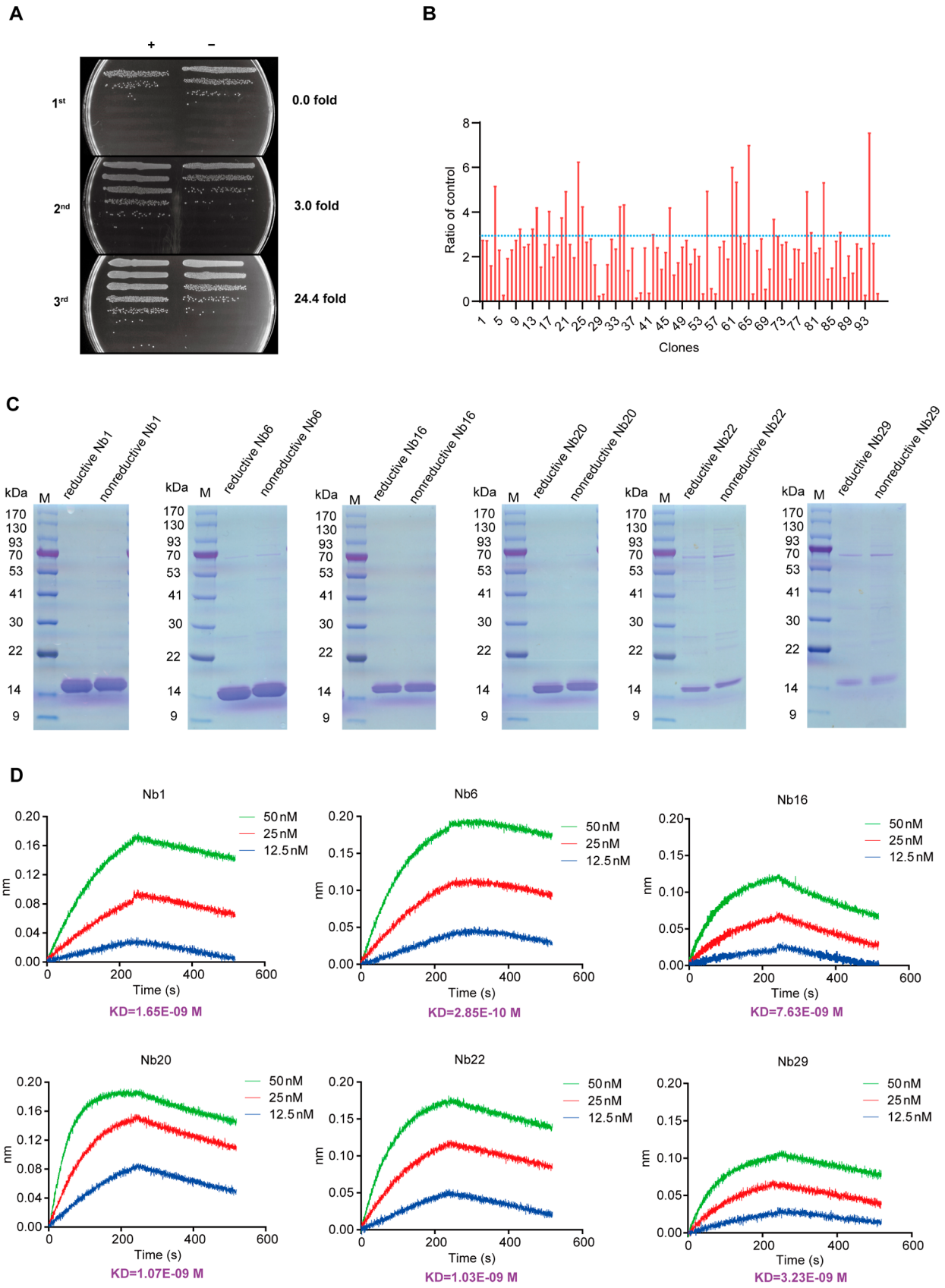

Figure 2. Apo-A1-specific Nbs were selected from phage display library and affinity determination. (A) The enrichment of phage particles was assessed following each round of panning. (B) The PE-ELISA was conducted for the identification of positive clones. (C) Analysis of six purified soluble anti-Apo-A1 Nbs by SDS−PAGE. (D) The affinity value of six Nbs toward Apo-A1.

https://doi.org/10.1021/acsami.4c14027
ACS Appl. Mater. Interfaces XXXX, XXX, XXX−XXX

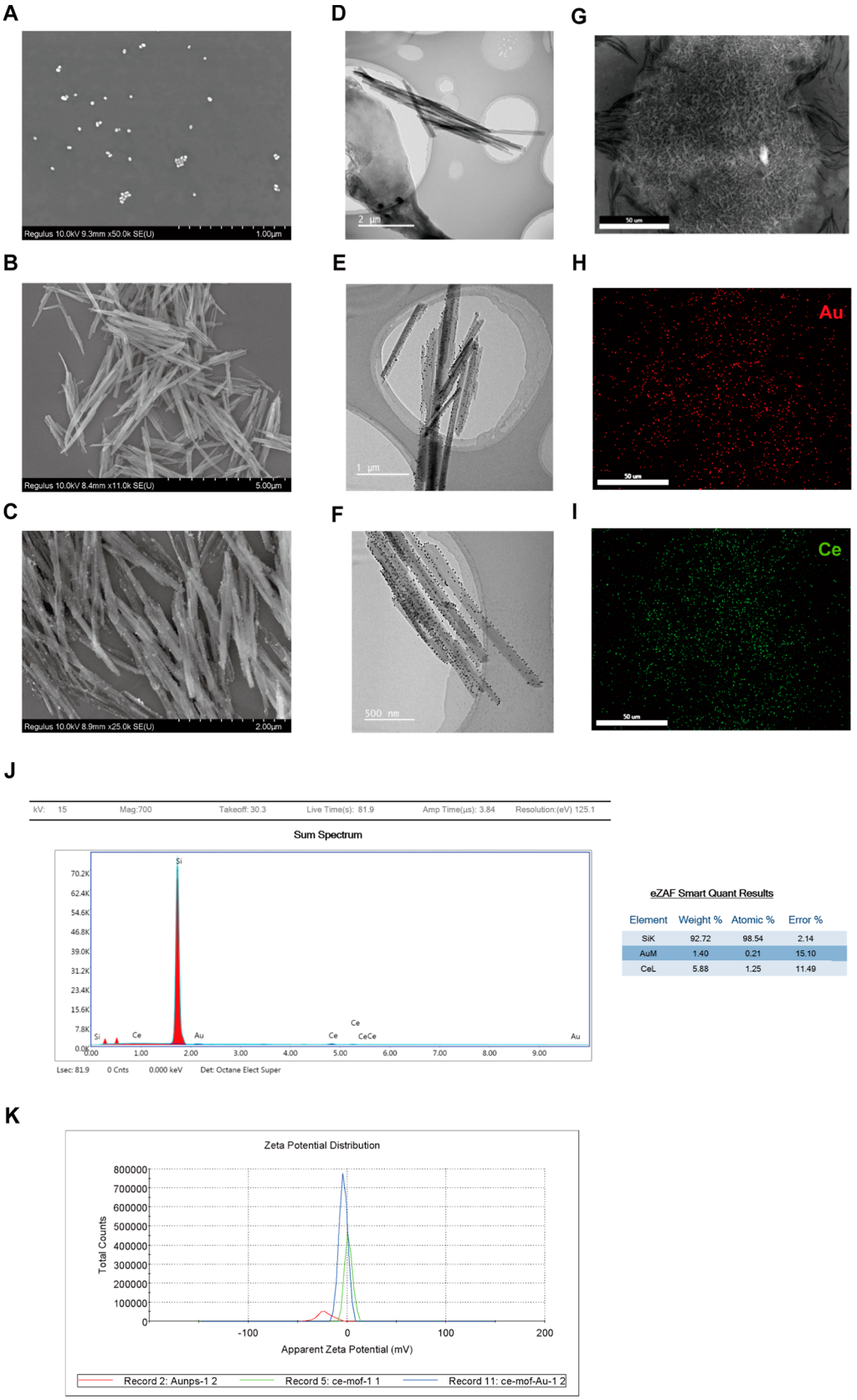

Figure 3. SEM and TEM diagram. (A) SEM images of AuNPs. (B) SEM images of Ce-MOF. (C) SEM images of Ce-MOF@Au. (D) TEM images of Ce-MOF. (E) TEM images of Ce-MOF@Au. (F) TEM picture with high magnification of Ce-MOF@Au. (G) SEM images of Ce-MOF@Au. (H) The corresponding mapping of the Au element of Ce-MOF@Au. (I) The corresponding mapping of the Ce element of Ce-MOF@Au. (J) The corresponding EDX mapping of Au and Ce elements. (K) Zeta potential study of AuNPs, Ce-MOF, and Ce-MOF@Au.

https://doi.org/10.1021/acsami.4c14027
ACS Appl. Mater. Interfaces XXXX, XXX, XXX−XXX

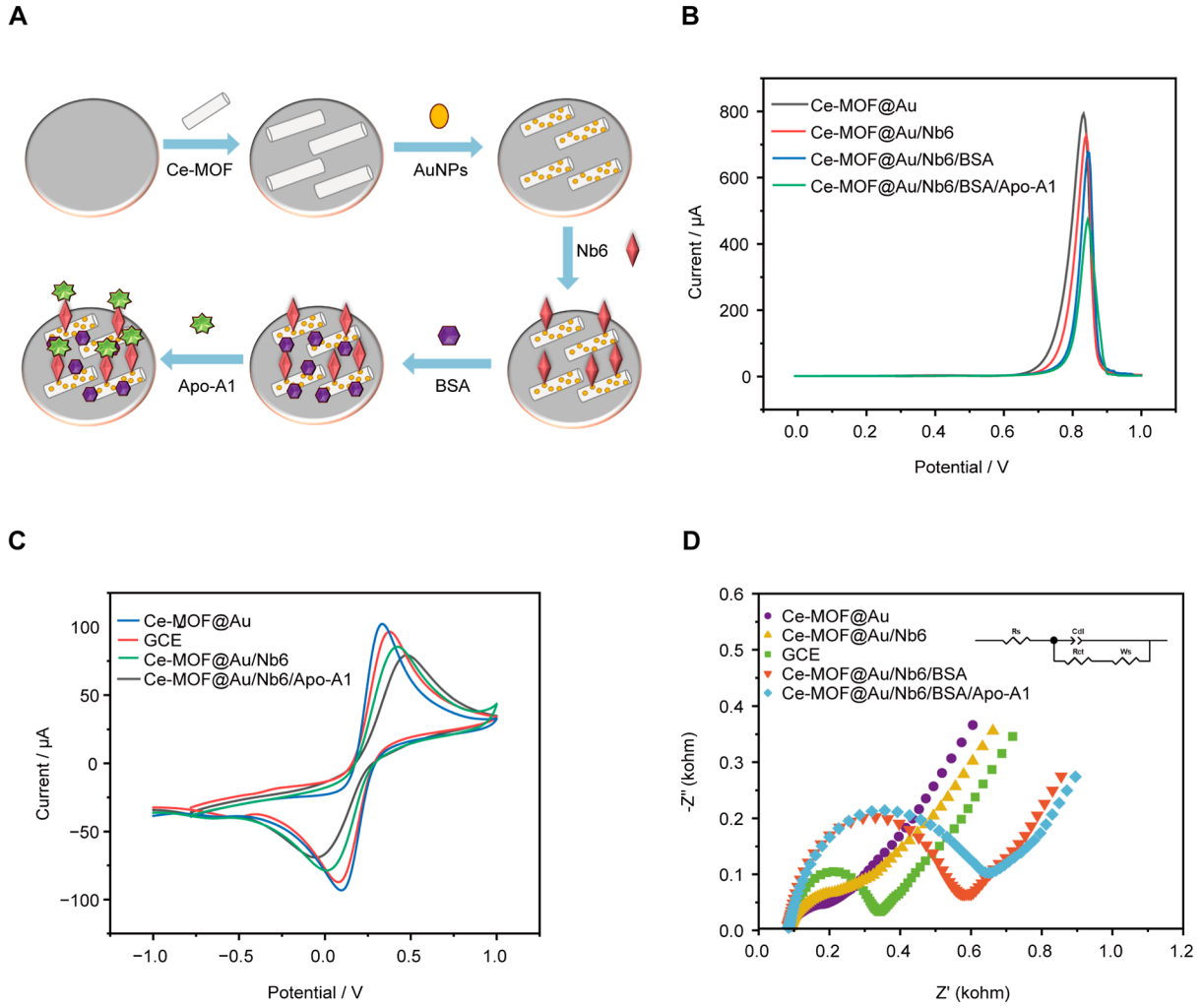

Figure 4. (A) Illustrated herein is a schematic depiction outlining the assembly procedure of the electrochemical biosensor. (B) The DPV in 0.2 M PBS (pH 7.3). (C) The CV in 0.1 mol/L KCl and 5 mmol/L $[Fe(CN)_6]^{-3/-4}$. (D) The EIS in 0.1 mol/L KCl and 5 mmol/L $[Fe(CN)_6]^{-3/-4}$.

the CDR3 region. These six Nbs were purified using Ni-NTA affinity columns, as confirmed by SDS-PAGE analysis (Figure 2C), showing molecular weights of approximately 15 kDa. The high purity of these Nbs was suitable for further research. The KD values of these Nbs for Apo-A1 are depicted in Figure 2D after affinity measurement. Affinity measurement showed that Nb6 had the highest affinity for Apo-A1, with a KD value of 2.85×10^{-10} M (Figure 2D), suggesting its potential for application in biosensors and diagnostic tools. Consequently, Nb6 was selected for further investigation.

Synthesis and Characterization of Ce-MOF@Au. SEM was employed to investigate the morphological attributes of the nanomaterials. The SEM images revealed spherical morphology characteristic of AuNPs, as depicted in Figure 3A.[43] Furthermore, SEM analysis elucidated that the Ce-MOF exhibits an elongated rod-like configuration measuring 4 to 5 μm in length and 300 to 400 nm in width, as illustrated in Figure 3B. Additionally, AuNPs were effectively synthesized on certain rod-like Ce-MOF structures (Figure 3C), confirming the successful fabrication of Ce-MOF@Au composite. The large surface area of Ce-MOF provides an extensive platform for immobilizing Nbs, thereby improving the antigen capture efficiency. Additionally, the integration of AuNPs improves the electron transfer, resulting in amplified electrochemical signals. Collectively, these factors contribute to the increased sensitivity and detection capabilities of the sensor.

TEM was used to conduct a detailed examination of the composition of Ce-MOF@Au. The results unveiled the successful synthesis of Ce-MOF (Figure 3D), showing a clear surface coating of AuNPs in different fields of view (Figure 3E,F). In summary, Ce-MOF@Au displayed a characteristic elongated rod morphology with prominent edge thickening and a rugged surface, accompanied by the deposition of numerous AuNPs on its surface.

The elemental composition of the Ce-MOF@Au composite was verified through elemental mapping, as illustrated in Figure 3G–J. The detection and distribution of elements, including Au and Ce, confirmed the successful synthesis of the Ce-MOF@Au composite.

The zeta potential study was conducted to characterize the surface charge of the MOF before and after functionalization. The zeta potential of AuNPs was approximately −26.4 mV, while the zeta potentials for Ce-MOF and Ce-MOF@Au were 1.42 and −5.57 mV (Figure 3K), respectively. The change in the zeta potential of Ce-MOF@Au compared to that of Ce-MOF and AuNPs suggests an interaction between these components, further indicating the successful formation of the composite.

https://doi.org/10.1021/acsami.4c14027
ACS Appl. Mater. Interfaces XXXX, XXX, XXX−XXX

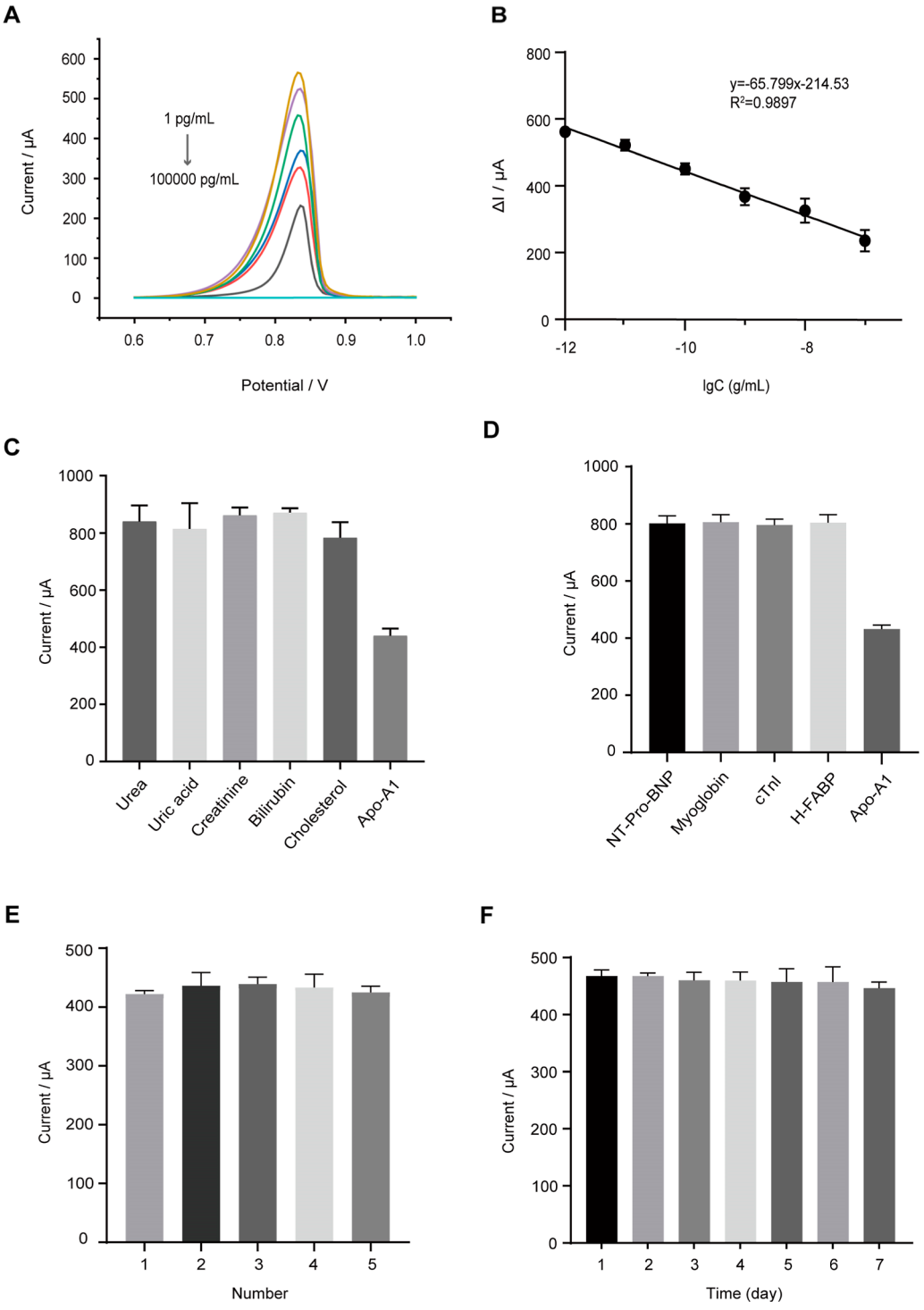

Figure 5. (A) Electrochemical response of the immunosensor with 1, 10, 100, 1000, 10,000, 100,000 pg/mL Apo-A1 under optimal conditions. (B) Calibration curve of the electrochemical immunosensor. (C) Specificity of the immunosensor investigated with 10 ng/mL urea, 10 ng/mL uric acid, 10 ng/mL creatinine, 10 ng/mL bilirubin, 10 ng/mL cholesterol, 1 ng/mLApo-A1. (D) Specificity of the immunosensor investigated with 10 ng/mL NT-Pro-BNP, 10 ng/mL myoglobin, 10 ng/mL cTnI, 10 ng/mL H-FABP, 1 ng/mL Apo-A1. (E) Reproducibility of different electrodes modified with 10 ng/mL of Apo-A1. (F) Stability of the sensor for different days.

Electrochemical Behavior. This study presents a label-free electrochemical immunoassay utilizing a Ce-MOF@Au multilayer nanocomposites for Apo-A1 detection (Figure 4A). DPV was employed to investigate the principles and characteristics of the electrochemical immunosensor in 0.2 M PBS solution at pH 7.3. A prominent electrical pulse at +0.8 V was observed following the introduction of Ce-MOF@Au multilayer nanocomposites (Figure 4B). Additionally, a marked reduction in this electrochemical signal occurred after immobilization of the antibody and antigen (Figure 4B). Consequently, the concentration of the Apo-A1 antigen can be quantified based on the variations at +0.8 V.

CV was employed to evaluate the electrochemical behavior, thereby assessing the preparation of the sensors. The CV

https://doi.org/10.1021/acsami.4c14027
ACS Appl. Mater. Interfaces XXXX, XXX, XXX−XXX

analysis was conducted in a solution comprising 0.1 mol/L KCl and 5 mmol/L $[Fe(CN)_6]^{-3/-4}$ (Figure 4C). The charge transfer resistance gradually decreased upon modification of electrodes with Ce-MOF@Au nanomaterials, attributed to the superior electrical conductivity of the nanocomposites. However, with the successive modification of Nb6, BSA, and Apo-A1 onto the electrodes, the electrochemical resistance increased during electron transfer, likely due to the repulsive effect exerted by self-adsorbed proteins. This observation suggests successful immobilization of Nb6, BSA, and Apo-A1 onto the electrode surface. Subsequently, following Nbs and Apo-A1 immobilization, the peak current intensity gradually diminished, indicative of the insulating properties inherent in biomolecules.

As depicted in Figure 4D, EIS was employed to assess the surface properties of the Ce-MOF@Au sensor and the assembly of Nb6 coupled to anti-Apo-A1. The EIS data was analyzed using a circuit model that included electron solution resistance (R_s), electron transfer resistance of the electrodes (R_{et}), double layer capacitance (C_{dl}), and Warburg impedance (W). As Ce-MOF@Au multilaminate nanocomposites were applied to the GCE surface, the resistance decreased significantly, demonstrating that the multilayer nanocomposites was secured to the electrodes. Due to the blocking effect of idioelectric proteins during electronic transfer, the electrochemical resistance increased as Nb6, BSA, and Apo-A1 were gradually changed onto the electrodes. This suggests that the electrodes had been successfully integrated with Nb6, BSA, and Apo-A1. Consistent results from both EIS and CV analyses confirm the successful establishment of the electrochemical immunosensor.

Optimization of Experimental Conditions. To enhance the analytical performance of the immunosensor, it was necessary to optimize the reaction parameters, including the concentration of Ce-MOF@Au, the concentration of Nb6 absorbed on Ce-MOF@Au, the incubation time for the antigen, and the pH.

First, the concentration of Ce-MOF@Au significantly affected the immunosensor's performance. As shown in Figure S1A, the peak current increased proportionally with the Ce-MOF@Au concentration from 0.2 to 1.0 mg/mL, reaching a maximum at 1.0 mg/mL, after which it gradually decreased. This decline was due to the saturation of Ce-MOF@Au adsorption on the GCE, indicating that an excessive amount of Ce-MOF@Au hindered the electron transfer rate at the electrode interface. Therefore, the optimal concentration of Ce-MOF@Au was determined to be 1.0 mg/mL.

In addition to Ce-MOF@Au concentration, the effect of Nbs concentration on the sensor's detection efficiency was also investigated. As shown in Figure S1B, the signal intensities were lowest at 10 μg/mL, likely due to increased electron transfer impedance caused by higher Nbs concentrations on the substrate. However, lower concentrations are more prone to operational errors. Therefore, 10 μg/mL was determined to be the optimal Nbs concentration.

Furthermore, the effect of the incubation time on sensor performance was examined. As the incubation period increased from 10 to 40 min, the peak current initially decreased. However, beyond this saturation point, extending the incubation time further may result in the dissociation of some complexes, leading to an increase in peak current when the incubation time was prolonged to 60 min (Figure S1C).[44] The decrease in peak current within the 10 to 40 min range suggests that saturated binding between Apo-A1 and anti-Apo-A1 Nbs occurred, indicating the formation of the maximum number of antibody−antigen immune complexes on the electrode surface. Consequently, the optimal incubation time for the experiment was determined to be 40 min.

Lastly, the pH significantly impacted the performance of the immunosensor. As shown in Figure S1D, acidic or alkaline PBS resulted in a reduction in the electrical signal. This effect is primarily attributed to the pH's impact on the activity of antigen and antibody, as well as their binding interactions. However, neutral conditions were found to be more favorable for the redox reactions of Ce-MOF@Au. Based on the optimization of conditions, the optimal pH for the experiment was determined to be 7.3.

Performance Evaluation of the Electrochemical Immunosensor. The immunosensor was assessed with varying concentrations of Apo-A1 standard solutions under the optimized conditions. DPV analysis showed a decrease in current response as Apo-A1 concentration increased (Figure 5A), attributed to the formation of immune complexes between Apo-A1 and Nb6. Furthermore, a well-defined linear relationship was established between the change in DPV current response (ΔI) and the logarithm of Apo-A1 concentration in the range of 1 to 100,000 pg/mL. The standard curve was defined as $I = 65.799 \log C - 214.53$, with a coefficient of determination (R^2) of 0.9897 (Figure 5B). The LOD was calculated to be 36 fg/mL from the calibration curve as LOD = $3s/b$, where s is the standard deviation of the intercept and b is the slope of the calibration curve.[45] These findings suggest that the proposed immunosensor exhibits an excellent performance for the quantitative detection of Apo-A1.

Selectivity, Reproducibility, and Stability of the Proposed Immunosensor. To assess the selectivity of the sensor, a range of common interfering antigens in blood, including urea, uric acid, creatinine, bilirubin, and cholesterol, were evaluated. The results showed a significant difference in the electrochemical signals between the interfering antigens (10 ng/mL) and the target antigen (1 ng/mL) (Figure 5C). Additionally, other cardiovascular disease markers, including NT-Pro-BNP, myoglobin, cTnI, and H-FABP, were also evaluated. The results indicated a significant difference in electrochemical signals between the interfering antigens (10 ng/mL) and the target antigen (1 ng/mL; Figure 5D). These findings demonstrated that the immunosensor exhibits enhanced selectivity.

To evaluate the reproducibility of the sensors, five electrochemical immunosensors were fabricated for the detection of Apo-A1 (10 ng/mL). The results revealed consistent electrical signal values across the five sensors upon repeated measurements, suggesting the robust reproducibility of the constructed electrochemical sensors (Figure 5E).

A series of electrodes was prepared and stored at 4 °C to evaluate the sensor's stability. After 7 days, the electrochemical signals generated by Ce-MOF@Au in the immunosensor decreased by less than 5% (Figure 5F). This minimal reduction in signal demonstrates the excellent stability of the electrochemical immunosensor over time.

A comparison with previous studies, as summarized in Table 1, highlights the advantages of our developed sensor. In contrast to the Ag-nHAP SPCE immunoassay, MoS_2/GOD/GCE immunoassay, and the MoS_2/ZrO_2/Naf-based ECL aptasensor targeting Apo-A1, our sensor constructed with a

https://doi.org/10.1021/acsami.4c14027
ACS Appl. Mater. Interfaces XXXX, XXX, XXX−XXX

Table 1. Comparison of the Performances of Different Apo-A1 Detection Methods

detection methods	linear range	LOD	reference
EC	0.1−50,000 pg/mL	0.02 pg/mL	46
EC	1.0−1,000,000 pg/mL	0.3 pg/mL	48
ECL	0.1−1000 pg/mL	53 fg/mL	47
ECL	100−10,000 pg/mL	50 pg/mL	49
ECL	1.0−1000 pg/mL	0.33 pg/mL	50
fluorescence spectroscopy	0.5−3.0 mg/mL	7.7 ng/mL	51
eELISA	1−100,000 pM	1.00 pM	53
colorimetric immunosensor	50−100,000 pg/mL	20 pg/mL	52
EC	0.1−1000 pg/mL	0.04 pg/mL	54
EC	1−100,000 pg/mL	36 fg/mL	this work

simpler direct binding approach using Nbs and antigens, along with more cost-effective Ce-MOF@Au materials, achieved comparable or superior detection ranges and limits than those in other studies.[46−48] Additionally, it outperformed these previous methods in terms of specificity and stability. Notably, the proposed immunosensor exhibited higher sensitivity and a broader linear range compared to previous works.[49−52] This improvement may be due to the use of Ce-MOFs, which possess good adsorption and adhesion properties, and are able to adsorb more AuNPs and provide more binding sites for Nbs immobilizations. As a result, the Nbs loading was greatly increased, allowing for the capture of more antigens and creating an optimal 3D environment for the construction of electrochemical immunosensors. Ce-MOF@Au improved both the electrical conductivity and Nbs loading capacity of the entire system, thereby significantly improving the sensitivity. Consequently, the developed electrochemical immunosensor demonstrated an excellent analytical performance for the detection of Apo-A1.

Application of the Immunosensor in Analyzing Clinical Samples. To validate the efficacy and precision of the immunosensor for real sample analysis, we assessed the recovery rates across varying concentrations of Apo-A1. As shown in Table 2, varied concentrations of Apo-A1 were introduced into serum samples (200 pg/mL), ranging from 10 to 500 pg/mL. The observed recoveries ranged from 101.9% to 107.11%, with relative standard deviations (RSD) between 1.30% and 3.50%.

Table 2. Recovery Experiment of the Electrochemical Sensor

blank sample concentration (pg/mL)	add (pg/mL)	total found (pg/mL)	recovery (%)	RSD (%)
200	10	219	106.67	2.23
		229		
		224		
	100	331	107.11	3.50
		324		
		309		
	500	708	101.9	1.30
		708		
		724		

Furthermore, Apo-A1 concentrations in human serum were evaluated using the developed immunosensor. To assess the method's accuracy, the relative error was calculated, demonstrating high concordance with the standard ELISA method (Table 3). The relative error for both methods ranged from 0.80% to 14.69%, indicating that the immunosensor is highly reliable and suitable for analyzing real human serum samples.

Table 3. Comparison of Apo-A1 Detection in Human Serum Samples Using Two Methods

serum sample	ELISA kit (ng/mL) (1/50,000 diluted)	present sensor (ng/mL) (1/50,000 diluted)	relative error (%)
1	24.57	26.98	9.80
2	8.17	9.37	14.69
3	5.01	4.97	−0.80
4	22.17	23.65	6.68
5	15.01	14.64	−2.47
6	17.62	16.34	−7.26

CONCLUSIONS

This investigation described a label-free electrochemical immunoassay utilizing Nbs and Ce-MOF@Au multilayer nanocomposites for the detection of Apo-A1. Due to their intrachain disulfide bonds, Nbs exhibit greater stability than mAbs, enabling them to withstand extreme pH conditions and elevated temperatures. The elongated and exposed convex complementary sites within the CDR3 region further enhance their binding affinity for target antigens. Additionally, the variable domain of Nbs significantly improves their solubility and diffusion in various matrices, while their small size reduces steric hindrance, promoting more efficient antigen binding and facilitating Nbs-antigen interactions. These distinctive features make Nbs a highly effective and versatile option for developing biosensors across a range of applications. In comparison to conventional MOF, Ce-MOF exhibit superior adsorption capacity and biocompatibility, making them ideal materials for electrode modification. Moreover, the synthesis of Ce-MOF using 1,3,5-benzenetricarboxylic acid as the organic framework is both efficient and straightforward, enhancing the feasibility of sensor construction. The porous rod-like architecture of Ce-MOF facilitates the adsorption of AuNPs, thereby increasing their conductivity and generating electrical signals. This Ce-MOF@Au electrochemical immunosensor exhibited a wide linear range, low LOD, and excellent stability, reproducibility, and selectivity. Additionally, the approach demonstrated in our study is applicable to various biosensors for detecting multiple disease biomarkers, pathogens, and toxins. The sensor's low cost, ease of fabrication, broad detection range, and high sensitivity highlight its significant potential for clinical applications. Leveraging the versatility of Nbs, we can tailor this platform for the detection of additional cardiovascular disease biomarkers. By incorporating specific Nbs targeting other biomarkers such as Apo-B or additional disease-related biomarkers, a multiplex diagnostic system can be established for the simultaneous assessment of multiple diseases and comorbidities. Through optimization of the electrochemical sensor's interface structure and refinement of detection methods, the platform can maintain high sensitivity while achieving the specificity required for multiplexed assays. This would significantly enhance diagnostic efficiency, providing a more comprehensive lipid profile and atherosclerosis risk assessment and thereby offering improved support for clinical diagnosis and personalized treatment.

https://doi.org/10.1021/acsami.4c14027
ACS Appl. Mater. Interfaces XXXX, XXX, XXX−XXX

Overall, engineered Nbs and Ce-MOF-based platforms exhibit potential for developing durable, cost-effective, and miniaturizable devices for detecting cardiovascular diseases biomarkers.

■ ASSOCIATED CONTENT

Supporting Information

The Supporting Information is available free of charge at https://pubs.acs.org/doi/10.1021/acsami.4c14027.

Optimization of experimental conditions to detect Apo-A1 (PDF)

■ AUTHOR INFORMATION

Corresponding Authors

Yakun Wan − *Shanghai Novamab Biopharmaceuticals Co, Ltd, Shanghai 201318, China*; Email: ykwan@novamab.com

Yanfei Li − *Shanghai University of Medicine & Health Sciences Affiliated Zhoupu Hospital, Shanghai 201318, China*; Email: liyf@sumhs.edu.cn

Linlin Ma − *Shanghai University of Medicine & Health Sciences Affiliated Zhoupu Hospital, Shanghai 201318, China*; orcid.org/0000-0002-5728-9509; Email: linlinma1986@gmail.com

Authors

Baihe Sun − *Shanghai University of Medicine & Health Sciences Affiliated Zhoupu Hospital, Shanghai 201318, China; School of Health Science and Engineering, University of Shanghai for Science and Technology, Shanghai 200093, China*

Guanghui Li − *Shanghai Novamab Biopharmaceuticals Co, Ltd, Shanghai 201318, China*

Yue Wu − *Shanghai University of Medicine & Health Sciences Affiliated Zhoupu Hospital, Shanghai 201318, China; School of Health Science and Engineering, University of Shanghai for Science and Technology, Shanghai 200093, China*

Junwei Gai − *Shanghai Novamab Biopharmaceuticals Co, Ltd, Shanghai 201318, China*

Min Zhu − *Shanghai Novamab Biopharmaceuticals Co, Ltd, Shanghai 201318, China*

Weiwei Ji − *Shanghai Novamab Biopharmaceuticals Co, Ltd, Shanghai 201318, China*

Xiaoying Wang − *School of Life Sciences and Technology, Tongji University, Shanghai 200092, China*

Fenghua Zhang − *Shanghai University of Medicine & Health Sciences Affiliated Zhoupu Hospital, Shanghai 201318, China*

Wanting Li − *Shanghai University of Medicine & Health Sciences Affiliated Zhoupu Hospital, Shanghai 201318, China*

Jingjin Hu − *Shanghai University of Medicine & Health Sciences Affiliated Zhoupu Hospital, Shanghai 201318, China*

Yuxin Lou − *Shanghai University of Medicine & Health Sciences Affiliated Zhoupu Hospital, Shanghai 201318, China*

Gusheng Feng − *Shanghai University of Medicine & Health Sciences Affiliated Zhoupu Hospital, Shanghai 201318, China*

Xijun Han − *Shanghai University of Medicine & Health Sciences Affiliated Zhoupu Hospital, Shanghai 201318, China*

Jinwen Dong − *Shanghai University of Medicine & Health Sciences Affiliated Zhoupu Hospital, Shanghai 201318, China*

Jiayuan Peng − *Shanghai University of Medicine & Health Sciences Affiliated Zhoupu Hospital, Shanghai 201318, China*

Jiawei Pei − *Shanghai University of Medicine & Health Sciences Affiliated Zhoupu Hospital, Shanghai 201318, China; School of Health Science and Engineering, University of Shanghai for Science and Technology, Shanghai 200093, China*

Complete contact information is available at: https://pubs.acs.org/10.1021/acsami.4c14027

Author Contributions

⊥B.S. and G.L. contribute equally.

Notes

The authors declare no competing financial interest.

Ethical Approval: The Clinical Research Ethics Committee at Shanghai University of Medicine & Health Sciences Affiliated Zhoupu Hospital has granted complete ethical approval for the utilization of human serum samples in this study. All animal experiments were approved by the Animal Experimental Ethics Committee of Shanghai University of Medicine and Health Sciences.

■ ACKNOWLEDGMENTS

This work was supported by Shanghai Innovation Fund Program (220H1209600), Science and Technology Commission of Shanghai Municipality (23J21901800), Biomedical Technology Support Special Project of "Shanghai Science and Technology Innovation Action Plan" (21S11901700), and Academic Mentorship for Scientific Research Cadre Project (AMSCP-22-05).

■ REFERENCES

(1) Oram, J. F.; Heinecke, J. W. Atp-Binding Cassette Transporter A1: A Cell Cholesterol Exporter That Protects against Cardiovascular Disease. *Physiol. Rev.* **2005**, *85* (4), 1343−1372.

(2) Walldius, G.; Jungner, I.; Holme, I.; Aastveit, A. H.; Kolar, W.; Steiner, E. High Apolipoprotein B, Low Apolipoprotein a-I, and Improvement in the Prediction of Fatal Myocardial Infarction (Amoris Study): A Prospective Study. *Lancet* **2001**, *358* (9298), 2026−2033.

(3) Májek, P.; Reicheltová, Z.; Suttnar, J.; Malý, M.; Oravec, M.; Pečánková, K.; Dyr, J. E. Plasma Proteome Changes in Cardiovascular Disease Patients: Novel Isoforms of Apolipoprotein A1. *J. Transl. Med.* **2011**, *9*, 84.

(4) Franceschini, G.; Sirtori, C. R.; Capurso, A., 2nd; Weisgraber, K. H.; Mahley, R. W. A-Imilano Apoprotein. Decreased High Density Lipoprotein Cholesterol Levels with Significant Lipoprotein Modifications and without Clinical Atherosclerosis in an Italian Family. *J. Clin. Invest.* **1980**, *66* (5), 892−900.

(5) Iwaoka, M.; Obata, J. E.; Abe, M.; Nakamura, T.; Kitta, Y.; Kodama, Y.; Kawabata, K.; Takano, H.; Fujioka, D.; Saito, Y.; Kobayashi, T.; Hasebe, H.; Kugiyama, K. Association of Low Serum Levels of Apolipoprotein a-I with Adverse Outcomes in Patients with Nonischemic Heart Failure. *J. Card. Failure* **2007**, *13* (4), 247−253.

(6) Wedel, H.; McMurray, J. J.; Lindberg, M.; Wikstrand, J.; Cleland, J. G.; Cornel, J. H.; Dunselman, P.; Hjalmarson, A.; Kjekshus, J.; Komajda, M.; Kuusi, T.; Vanhaecke, J.; Waagstein, F.; Group, C. S. Predictors of Fatal and Non-Fatal Outcomes in the Controlled Rosuvastatin Multinational Trial in Heart Failure (Corona): Incremental Value of Apolipoprotein a-1, High-Sensitivity C-Reactive

Peptide and N-Terminal Pro B-Type Natriuretic Peptide. *Eur. J. Heart Failure* **2009**, *11* (3), 281−291.
(7) Li, C.; Li, H.; Zhang, T.; Li, J.; Liu, L.; Chang, J. Discovery of Apo-A1 as a Potential Bladder Cancer Biomarker by Urine Proteomics and Analysis. *Biochem. Biophys. Res. Commun.* **2014**, *446* (4), 1047−1052.
(8) Wang, X. L.; Dudman, N. P.; Blades, B. L.; Wilcken, D. E. Changes in the Immunoreactivity of Apo a-I During Storage. *Clin. Chim. Acta* **1989**, *179* (3), 285−293.
(9) Wang, X. L.; Wilcken, D. E.; Dudman, N. P. Neonatal Apo a-I, Apo B, and Apo(a) Levels in Dried Blood Spots in an Australian Population. *Pediatr. Res.* **1990**, *28* (5), 496−501.
(10) Ikeda, T.; Shibuya, Y.; Senba, U.; Sugiuchi, H.; Araki, S.; Uji, Y.; Okabe, H. Automated Immunoturbidimetric Analysis of Six Plasma Apolipoproteins: Correlation with Radial Immunodiffusion Assays. *J. Clin. Lab. Anal.* **1991**, *5* (2), 90−95.
(11) He, H.; Feng, J.; Zhang, S.; Wang, Y.; Li, J.; Gao, J.; Cong, J.; Gong, Y.; Wu, X. The Apolipoprotein B/A1 Ratio Is Associated with Metabolic Syndrome Components, Insulin Resistance, Androgen Hormones, and Liver Enzymes in Women with Polycystic Ovary Syndrome. *Front. Endocrinol.* **2022**, *12*, 12773781.
(12) van den Broek, I.; Romijn, F. P.; Nouta, J.; van der Laarse, A.; Drijfhout, J. W.; Smit, N. P.; van der Burgt, Y. E.; Cobbaert, C. M. Automated Multiplex Lc-Ms/Ms Assay for Quantifying Serum Apolipoproteins a-I, B, C-I, C-Ii, C-Iii, and E with Qualitative Apolipoprotein E Phenotyping. *Clin. Chem.* **2016**, *62* (1), 188−197.
(13) Kay, R. G.; Gregory, B.; Grace, P. B.; Pleasance, S. The Application of Ultra-Performance Liquid Chromatography/Tandem Mass Spectrometry to the Detection and Quantitation of Apolipoproteins in Human Serum. *Rapid Commun. Mass Spectrom.* **2007**, *21* (16), 2585−2593.
(14) Velayudham, J.; Magudeeswaran, V.; Paramasivam, S. S.; Karruppaya, G.; Manickam, P. Hydrogel-Aptamer Nanocomposite Based Electrochemical Sensor for the Detection of Progesterone. *Mater. Lett.* **2021**, *305*, 305130801.
(15) Balkourani, G.; Brouzgou, A.; Archonti, M.; Papandrianos, N.; Song, S.; Tsiakaras, P. Emerging Materials for the Electrochemical Detection of Covid-19. *J. Electroanal. Chem.* **2021**, *893*, 893115289.
(16) Li, J.; Cai, R.; Tan, W. A Novel Ecl Sensing System for Ultrahigh Sensitivity Mirna-21 Detection Based on Catalytic Hairpin Assembly Cascade Nonmetallic Spr Effect. *Anal. Chem.* **2022**, *94* (36), 12280−12285.
(17) Wu, K.; Chen, R.; Zhou, Z.; Chen, X.; Lv, Y.; Ma, J.; Shen, Y.; Liu, S.; Zhang, Y. Elucidating Electrocatalytic Oxygen Reduction Kinetics Via Intermediates by Time-Dependent Electrochemiluminescence. *Angew. Chem., Int. Ed. Engl.* **2023**, *135* (12), No. e202217078.
(18) Peng, Y.; Shang, H.; Zheng, Z.; Li, H.; Chen, W.; Xu, J. Self-Activation of Symbiotic Multi-DNA Machines Transducing Exponentially Amplified Fluorescence for Ultrasensitively Signaling of Terminal Deoxynucleotidyl Transferase Activity. *Sens. Actuators, B* **2023**, *380*, 380133400.
(19) Miyazaki, O.; Ogihara, J.; Fukamachi, I.; Kasumi, T. Evidence for the Presence of Lipid-Free Monomolecular Apolipoprotein a-1 in Plasma. *J. Lipid Res.* **2014**, *55* (2), 214−225.
(20) Wang, B.; He, B.; Guo, R.; Jiao, Q.; Liang, Y.; Wang, J.; Liu, Y.; Ren, W.; Suo, Z. A Competitive-Type Electrochemical Immunosensor Based on Ce-Mof@Au and Mb-Au@Pt Core-Shell for Nitrofuran Metabolites Residues Detection. *Bioelectrochemistry* **2021**, *142*, 142107934.
(21) Xiong, Y.; Chen, S.; Ye, F.; Su, L.; Zhang, C.; Shen, S.; Zhao, S. Synthesis of a Mixed Valence State Ce-Mof as an Oxidase Mimetic for the Colorimetric Detection of Biothiols. *Chem. Commun.* **2015**, *51* (22), 4635−4638.
(22) Li, W.; Ma, C.; Song, Y.; Hong, C.; Qiao, X.; Yin, B. Sensitive Detection of Carcinoembryonic Antigen (Cea) by a Sandwich-Type Electrochemical Immunosensor Using Mof-Ce@Ha/Ag-Hrp-Ab(2) as a Nanoprobe. *Nanotechnology* **2020**, *31* (18), 185605.
(23) Fu, X.; He, J.; Zhang, C.; Chen, J.; Wen, Y.; Li, J.; Mao, W.; Zhong, H.; Wu, J.; Ji, X.; Yu, C. Trimetallic Signal Amplification Aptasensor for Tsp-1 Detection Based on Ce-Mof@Au and Auptru Nanocomposites. *Biosens. Bioelectron.* **2019**, *132*, 132302−132309.
(24) Shen, W. J.; Zhuo, Y.; Chai, Y. Q.; Yuan, R. Ce-Based Metal-Organic Frameworks and Dnazyme-Assisted Recycling as Dual Signal Amplifiers for Sensitive Electrochemical Detection of Lipopolysaccharide. *Biosens. Bioelectron.* **2016**, *83*, 83287−83292.
(25) Baker, M. Reproducibility crisis: Blame it on the antibodies. *Nature* **2015**, *521* (7552), 274−276.
(26) Yu, X.; Xu, Q.; Wu, Y.; Jiang, H.; Wei, W.; Zulipikaer, A.; Guo, Y.; Jirimutu.Chen, J.; Chen, J. Nanobodies Derived from Camelids Represent Versatile Biomolecules for Biomedical Applications. *Biomater. Sci.* **2020**, *8* (13), 3559−3573.
(27) De Meyer, T.; Muyldermans, S.; Depicker, A. Nanobody-Based Products as Research and Diagnostic Tools. *Trends Biotechnol.* **2014**, *32* (5), 263−270.
(28) Li, H.; Mu, Y.; Yan, J.; Cui, D.; Ou, W.; Wan, Y.; Liu, S. Label-Free Photoelectrochemical Immunosensor for Neutrophil Gelatinase-Associated Lipocalin Based on the Use of Nanobodies. *Anal. Chem.* **2015**, *87* (3), 2007−2015.
(29) Zhou, Q.; Li, G.; Zhang, Y.; Zhu, M.; Wan, Y.; Shen, Y. Highly Selective and Sensitive Electrochemical Immunoassay of Cry1c Using Nanobody and Π-Π Stacked Graphene Oxide/Thionine Assembly. *Anal. Chem.* **2016**, *88* (19), 9830−9836.
(30) Yong Joon Kim, J.; Sang, Z.; Xiang, Y.; Shen, Z.; Shi, Y. Nanobodies: Robust Miniprotein Binders in Biomedicine. *Adv. Drug Delivery Rev.* **2023**, *195*, 195114726.
(31) Jin, B. K.; Odongo, S.; Radwanska, M.; Magez, S. NANOBODIES®: A Review of Diagnostic and Therapeutic Applications. *Int. J. Mol. Sci.* **2023**, *24* (6), 5994.
(32) Verkhivker, G. Structural and Computational Studies of the Sars-Cov-2 Spike Protein Binding Mechanisms with Nanobodies: From Structure and Dynamics to Avidity-Driven Nanobody Engineering. *Int. J. Mol. Sci.* **2022**, *23* (6), 2928.
(33) Cruz-Pacheco, A. F.; Monsalve, Y.; Serrano-Rivero, Y.; Salazar-Uribe, J.; Moreno, E.; Orozco, J. Engineered Synthetic Nanobody-Based Biosensors for Electrochemical Detection of Epidermal Growth Factor Receptor. *Chem. Eng. J.* **2023**, *465*, 465142941.
(34) Dumoulin, M.; Conrath, K.; Van Meirhaeghe, A.; Meersman, F.; Heremans, K.; Frenken, L. G.; Muyldermans, S.; Wyns, L.; Matagne, A. Single-Domain Antibody Fragments with High Conformational Stability. *Protein Sci.* **2002**, *11* (3), 500−515.
(35) Liu, X.; Wen, Y.; Wang, W.; Zhao, Z.; Han, Y.; Tang, K.; Wang, D. Nanobody-Based Electrochemical Competitive Immunosensor for the Detection of Afb1 through Afb1-Hcr as Signal Amplifier. *Mikrochim. Acta* **2020**, *187* (6), 352.
(36) Arshavsky-Graham, S.; Heuer, C.; Jiang, X.; Segal, E. Aptasensors Versus Immunosensors-Which Will Prevail? *Eng. Life Sci.* **2022**, *22* (3−4), 319−333.
(37) Zhang, M.; Chen, D.; Fu, X.; Meng, H.; Nan, F.; Sun, Z.; Yu, H.; Zhang, L.; Li, L.; Li, X.; Wang, X.; Wang, M.; You, F.; Li, Z.; Chang, Y.; Zhou, Z.; Yan, J.; Li, J.; Wu, X.; Wang, Y.; Wang, Y.; Xiang, S.; Chen, Y.; Pan, G.; Xu, H.; Zhang, B.; Yang, L. Autologous Nanobody-Derived Fratricide-Resistant Cd7-Car T-Cell Therapy for Patients with Relapsed and Refractory T-Cell Acute Lymphoblastic Leukemia/Lymphoma. *Clin. Cancer Res.* **2022**, *28* (13), 2830−2843.
(38) Muyldermans, S. Applications of Nanobodies. *Annu. Rev. Anim. Biosci.* **2021**, *9*, 9401−9421.
(39) Ma, L.; Zhu, M.; Gai, J.; Li, G.; Chang, Q.; Qiao, P.; Cao, L.; Chen, W.; Zhang, S.; Wan, Y. Preclinical Development of a Novel Cd47 Nanobody with Less Toxicity and Enhanced Anti-Cancer Therapeutic Potential. *J. Nanobiotechnol.* **2020**, *18* (1), 12.
(40) Xian, Z.; Ma, L.; Zhu, M.; Li, G.; Gai, J.; Chang, Q.; Huang, Y.; Ju, D.; Wan, Y. Blocking the Pd-1-Pd-L1 Axis by a Novel Pd-1 Specific Nanobody Expressed in Yeast as a Potential Therapeutic for Immunotherapy. *Biochem. Biophys. Res. Commun.* **2019**, *519* (2), 267−273.

https://doi.org/10.1021/acsami.4c14027
ACS Appl. Mater. Interfaces XXXX, XXX, XXX−XXX

(41) Zhu, M.; Hu, Y.; Li, G.; Ou, W.; Mao, P.; Xin, S.; Wan, Y. Combining Magnetic Nanoparticle with Biotinylated Nanobodies for Rapid and Sensitive Detection of Influenza H3n2. *Nanoscale Res. Lett.* **2014**, *9* (1), 528.
(42) Zhu, M.; Gong, X.; Hu, Y.; Ou, W.; Wan, Y. Streptavidin-Biotin-Based Directional Double Nanobody Sandwich Elisa for Clinical Rapid and Sensitive Detection of Influenza H5n1. *J. Transl. Med.* **2014**, *12*, 12352.
(43) Wen, X. H.; Zhao, X. F.; Peng, B. F.; Yuan, K. P.; Li, X. X.; Zhu, L. Y.; Lu, H. L. Facile Preparation of an Electrochemical Aptasensor Based on Au Nps/Graphene Sponge for Detection of Homocysteine. *Appl. Surf. Sci.* **2021**, *556*, 556149735.
(44) Zhu, L.; Dong, X.; Gao, C.; Gai, Z.; He, Y.; Qian, Z.; Liu, Y.; Lei, H.; Sun, Y.; Xu, Z. Development of a Highly Sensitive and Selective Electrochemical Immunosensor for Controlling of Rhodamine B Abuse in Food Samples. *Food Control* **2022**, *133*, 133108662.
(45) Ermer, J.; Miller, J. H. M. *Method Validation in Pharmaceutical Analysis*; Wiley-VCH Pub, 2005.
(46) Wang, H.; Li, G.; Zhang, Y.; Zhu, M.; Ma, H.; Du, B.; Wei, Q.; Wan, Y. Nanobody-Based Electrochemical Immunoassay for Ultrasensitive Determination of Apolipoprotein-A1 Using Silver Nanoparticles Loaded Nanohydroxyapatite as Label. *Anal. Chem.* **2015**, *87* (22), 11209−11214.
(47) Kurup, C. P.; Mohd-Naim, N. F.; Keasberry, N. A.; Zakaria, S. N. A.; Bansal, V.; Ahmed, M. U. Label-Free Electrochemiluminescence Nano-Aptasensor for the Ultrasensitive Detection of Apoa1 in Human Serum. *ACS Omega* **2022**, *7* (43), 38709−38716.
(48) Zhang, X.; Qi, J.; Zhang, Q.; Xue, Y.; Meng, F.; Zhang, J.; Liu, Y.; Yang, G.; Wu, C. A novel sandwich impedimetric immunosensor for detection of apolipoprotein-A1 based on the gold nanoparticle−hybridized mercapto-β-cyclodextrin-Pb(II) metal−organic framework. *Mikrochim. Acta* **2022**, *190* (1), 33.
(49) Zhang, S.; Huang, F.; Liu, B.; Ding, J.; Xu, X.; Kong, J. A Sensitive Impedance Immunosensor Based on Functionalized Gold Nanoparticle-Protein Composite Films for Probing Apolipoprotein a-I. *Talanta* **2007**, *71* (2), 874−881.
(50) Zhou, Y.; Yu, Y.; Chai, Y. Q.; Yuan, R. Electrochemical Synthesis of Silver Nanoclusters on Electrochemiluminescent Resonance Energy Transfer Amplification Platform for Apo-A1 Detection. *Talanta* **2018**, *181*, 18132−18137.
(51) Pal, M. K.; Rashid, M.; Bisht, M. Multiplexed Magnetic Nanoparticle-Antibody Conjugates (Mnps-Abs) Based Prognostic Detection of Ovarian Cancer Biomarkers, Ca-125, B-2m and Apoa1 Using Fluorescence Spectroscopy with Comparison of Surface Plasmon Resonance (Spr) Analysis. *Biosens. Bioelectron.* **2015**, *73*, 73146−73152.
(52) Peng, C.; Hua, M. Y.; Li, N. S.; Hsu, Y. P.; Chen, Y. T.; Chuang, C. K.; Pang, S. T.; Yang, H. W. A Colorimetric Immunosensor Based on Self-Linkable Dual-Nanozyme for Ultrasensitive Bladder Cancer Diagnosis and Prognosis Monitoring. *Biosens. Bioelectron.* **2019**, *126*, 126581−126589.
(53) Kim, S. E.; Kim, Y. J.; Song, S.; Lee, K. N.; Seong, W. K. A Simple Electrochemical Immunosensor Platform for Detection of Apolipoprotein A1 (Apo-A1) as a Bladder Cancer Biomarker in Urine. *Sens. Actuators, B* **2019**, *278*, 278103−278109.
(54) Husna, R.; Kurup, C. P.; Ansari, M. A.; Mohd-Naim, N. F.; Ahmed, M. U. An Electrochemical Aptasensor Based on Aunrs/Aunws for Sensitive Detection of Apolipoprotein a-1 (Apoa1) from Human Serum. *RSC Adv.* **2023**, *13* (6), 3890−3898.

https://doi.org/10.1021/acsami.4c14027
ACS Appl. Mater. Interfaces XXXX, XXX, XXX−XXX